CHEMISTRY
AN ASIAN JOURNAL

DOI: 10.1002/asia.200700054

VIP

Single-Crystalline and Near-Monodispersed $NaMF_3$ (M = Mn, Co, Ni, Mg) and $LiMAlF_6$ (M = Ca, Sr) Nanocrystals from Cothermolysis of Multiple Trifluoroacetates in Solution

Ya-Ping Du, Ya-Wen Zhang,* Zheng-Guang Yan, Ling-Dong Sun, Song Gao, and Chun-Hua Yan*[a]

Abstract: We report the synthesis of single-crystalline and near-monodispersed $NaMF_3$ (M = Mn, Co, Ni, Mg), $LiMAlF_6$ (M = Ca, Sr), and $NaMgF_3$:Yb,Er nanocrystals (quasisquare nanoplates, nanorods, and nanopolygons) by the cothermolysis of multiple trifluoroacetates in hot combined organic solvents (oleic acid, oleylamine, and 1-octadecene). The nanocrystals were characterized by XRD, TEM, superconductive quantum interference device (SQUID), and upconversion luminescence spectroscopy. By regulating the polarity of the dispersant, the $NaMF_3$ (M = Mn, Co, Ni) nanoplates were partially aligned to form nanoarrays on copper TEM grids. The sizes of the $NaMF_3$ nanocrystals were easily tuned by the use of proper synthetic conditions such as reaction temperature and time and solvent composition. On the basis of a series of experiments in which the reaction conditions were varied, together with GC–MS and FTIR analysis, the reaction pathways for the formation of these nanocrystals from trifluoroacetate precursors were proposed. The magnetic measurements showed that the differently sized $NaMnF_3$ square plates displayed interesting weak ferromagnetic behavior on the nanometer scale. The strong red upconversion luminescence emitted from the $NaMgF_3$:Yb,Er nanorods under 980-nm near-IR laser excitation suggests that $NaMgF_3$ may be a good candidate host material for red upconversion luminescence.

Keywords: crystal growth · fluorescence · fluorides · nanostructures · synthetic methods

Introduction

During the past two decades, research into novel inorganic materials with nanoscale dimensions has undergone tremendous progress, much of it due to the fact that unique properties are acquired on this scale with respect to their bulk counterparts.[1] An increasingly active part of this field is the delicate control of the shape and size of dispersible colloid inorganic nanocrystals driven by their interesting size- and shape-dependent properties, as well as the assembly of advanced materials and devices by using nanoscale building blocks.[2] Until now, much effort has been made in pursuing effective and robust means of manipulating the size and shape of nanocrystals such as semiconductors,[3] metals,[1d,e,4] alloys,[5] and metal oxides.[1g,2c,d,6] Moreover, their size- and shape-dependent properties give them promising applications in many fields, such as optics, electrics, magnetics, catalysis, and biosensing, that are of both fundamental and technological importance.[1a,b,2]

As important inorganic functional materials, complex metal fluorides such as $A^IM^{II}F_3$ and $A^IM^{II}M^{III}F_6$ have attracted much attention owing to their physical and chemical properties, such as ferromagnetism,[7] behavior as nonmagnetic insulators,[8] and piezoelectric characteristics,[9] as well as their optical properties.[10] It is widely accepted that nanoscaled materials have opened the doors for finding new properties with respect to their macroscopic counterparts. For example, for small antiferromagnetic particles such as alkaline fluoromanganates, net magnetization originating

[a] Y.-P. Du, Prof. Dr. Y.-W. Zhang, Dr. Z.-G. Yan, Prof. Dr. L.-D. Sun, Prof. Dr. S. Gao, Prof. Dr. C.-H. Yan
Beijing National Laboratory for Molecular Sciences
State Key Laboratory of Rare Earth Materials Chemistry and Applications
PKU-HKU Joint Laboratory in Rare Earth Materials and Bioinorganic Chemistry
Peking University, Beijing 100871 (China)
Fax: (+86) 10-6275-4179
E-mail: yan@pku.edu.cn
ywzhang@pku.edu.cn

Supporting information for this article is available on the WWW under http://www.chemasianj.org or from the author.

from the noncompensation of surface spins is observed below the ordering temperature owing to the high surface/volume ratio of these particles.[11] Recent work disclosed that $KMnF_3$ nanocrystals undergo a transition from paramagnetic to antiferromagnetic at 88.3 K.[11]

However, to date, very few studies have been done in the field of complex metal fluoride nanocrystals, partly because the conventional synthetic routes for these compounds are limited and complicated. For example, high-temperature solid-state synthesis requires apparatus with an intricate setup because of the chemical sensitivity between oxygen and fluoride and the corrosive nature of fluorine,[12] wet chemical synthetic strategies such as the hydrothermal method produce nanocrystals with nonuniform shape and size,[13] and the reversed micelle method usually involves onerous posttreatment procedures.[11] Therefore, the development of an effective synthetic route towards high-quality complex metal fluoride nanocrystals of tunable size that avoids these drawbacks still remains a challenge.

Recently, many successful methods have been found for the fabrication of high-quality dispersible colloid nanocrystals, among which are various nonhydrolytic synthetic pathways that use organometallic precursors in hot solvents with high boiling points. These conditions permit a relatively facile and reproducible approach for such nanocrystals that are single-crystalline, phase-pure, and monodispersed.[3a,14] Therefore, the determination of suitable molecular precursors, the adjustment of the capping ability of solvents, and the balance of the nucleation and growth stages are three key factors for the preparation of high-quality nanocrystals. Lately, our group developed an effective and general solution-phase route to prepare high-quality rare-earth fluoride and sodium rare-earth fluoride nanocrystals from trifluoroacetate precursors.[14e,g,h]

Herein, we report the one-pot synthesis of single-crystalline and monodispersed $NaMF_3$ (M = Mn, Co, Ni, Mg), $LiMAlF_6$ (M = Ca, Sr), and $NaMgF_3$:Yb,Er nanocrystals (quasisquare nanoplates, nanorods, and nanopolygons) by the cothermolysis of multiple trifluroacetates in hot combined organic solvents that include oleic acid (OA), oleylamine (OM), and 1-octadecene (ODE). The mechanism of the controlled synthesis as well as the magnetic and optical properties of the nanocrystals are also presented in this paper.

Abstract in Chinese:

通过多种金属三氟乙酸盐前驱体在高沸点混合溶剂(油酸、油胺和十八烯)中的热分解反应，合成了尺寸均一、形貌可控(纳米准四方板、纳米棒和纳米多面体)的 $NaMF_3$ (M = Mn, Co, Ni, Mg)、$LiMAlF_6$ (M = Ca, Sr)和 $NaMgF_3$:Yb,Er 单晶纳米颗粒。采用 X 射线衍射(XRD)、透射电子显微镜(TEM)、超导量子干涉仪(SQUID)和近红外激发光谱对所得纳米晶进行了结构、磁性和上转换发光性质表征。以气相色谱质谱联用(GC-MS)和傅立叶转换红外光谱(FTIR)对反应过程进行了监测，研究了反应历程和纳米晶的生成机理。研究结果表明，控制反应温度、时间和溶剂组成等条件，可以有效地控制纳米晶的尺寸；$NaMnF_3$ 四方板呈现与纳米尺寸相关的弱铁磁行为；$NaMgF_3$:Yb,Er 纳米晶在 980 nm 近红外激光激发下具有显著的上转换特性。

Results and Discussion

Characterization of $NaMF_3$ Nanocrystals

The XRD profiles in Figure 1 show that all the reflections for the $NaMF_3$ (M = Mn, Co, Ni, Mg) nanocrystals can be indexed to a pure orthorhombic phase (space group: *Pnma*). The calculated lattice constants are as follows: $a = 5.75(0)$ Å, $b = 8.00(4)$ Å, and $c = 5.55(1)$ Å for $NaMnF_3$ (JCPDS: 18–1224), $a = 5.35(1)$ Å, $b = 7.71(5)$ Å, and $c = 5.52(5)$ Å for $NaNiF_3$ (JCPDS: 70–2401), $a = 5.61(5)$ Å, $b = 7.78(5)$ Å, and $c = 5.41(9)$ Å for $NaCoF_3$ (JCPDS: 70–1889), and $a = 5.37(3)$ Å, $b = 5.48(5)$ Å, and $c = 7.67(1)$ Å for $NaMgF_3$ (JCPDS: 82–1226). The moderate sharpening of the diffraction peaks suggests the high crystallinity and large sizes of the $NaMF_3$ nanocrystals formed.

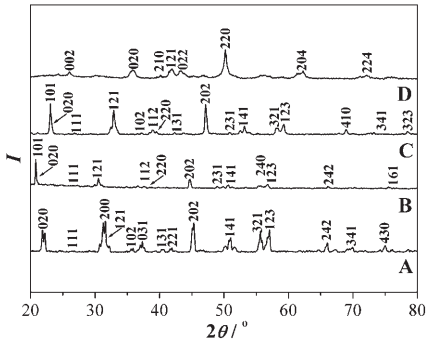

Figure 1. XRD patterns of orthorhombic $NaMnF_3$ (A), $NaCoF_3$ (B), $NaNiF_3$ (C), and $NaMgF_3$ (D) nanocrystals.

Energy dispersive X-ray (EDAX) analysis shows that the atomic ratios of Na to M (M = Mn, Co, Ni, Mg) determined are in good agreement with the expected values, thus indicating the formation of stoichiometric $NaMF_3$ compounds (see Supporting Information, Figure S1). The TEM and high-resolution TEM (HRTEM) images reveal that the $NaMF_3$ (M = Mn, Co, Ni) nanocrystals take on a quasi-square-plate shape (Figure 2), but the $NaMgF_3$ nanocrystals are rod-shaped (Figure 3). By delicate adjustment of the polarity of the dispersant, the $NaMF_3$ (M = Mn, Co, Ni) nanocrystals formed partially ordered arrays on the TEM grids, either lying flat on the face (Figure 2a, c, e) or standing on the edge (Figure 2b, d, f), which is indicative of the presence of capping ligands on the surfaces of the nanocrystals. Figure 2a, c, e shows the quasi-2D arrangement of $NaMnF_3$, $NaNiF_3$, and $NaCoF_3$ nanoplates, respectively, lying flat on the face as deposited from nanocrystal dispersion in toluene/hexane (1:1 *v*/*v*). As seen in Figure 2a–f, the clear lattice fringes shown in the HRTEM images reveal that the lattice planes of the nanocrystals afforded are perfectly aligned and

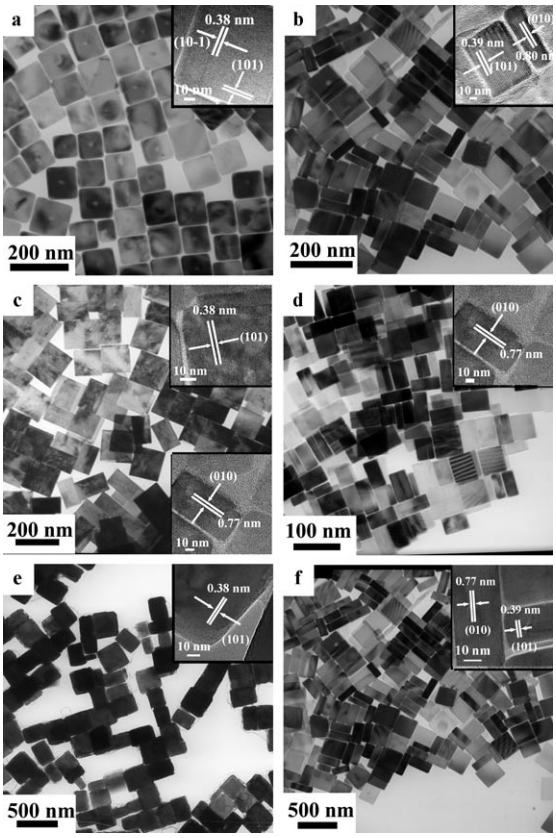

Figure 2. TEM and HRTEM (inset) images of $NaMnF_3$ (a = lying flat on the face, b = standing on the edge), $NaNiF_3$ (c = lying flat on the face, d = standing on the edge), and $NaCoF_3$ (e = lying flat on the face, f = standing on the edge) nanoplates.

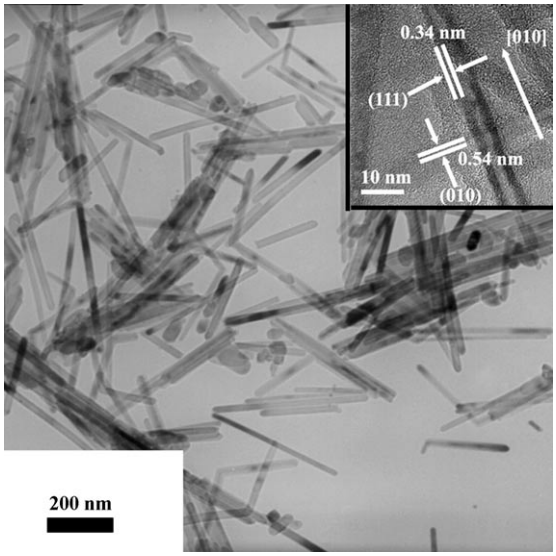

Figure 3. TEM and HRTEM (inset) images of $NaMgF_3$ nanorods.

go right through the entire nanoplate, thus confirming the single-crystalline nature of the nanocrystals without any stacking faults. From the HRTEM image in Figure 2a, inset, the interplanar spacing of 0.38 nm ascribed to the {101} face is found on the top surface of the $NaMnF_3$ nanoplates. When the polarity of the dispersant was increased by the addition of ethanol (toluene/hexane/ethanol = 1:1:2), the nanoplates were arranged almost in the face-to-face formation, unfolded by the {010} faces, on the copper TEM grids (Figure 2b). The {101} and {010} faces enclose the $NaMnF_3$ nanoplates, which are $(110.0 \pm 9.5) \times (40.5 \pm 2.0)$ nm^2 large. Similarly, the $NaNiF_3$ and $NaCoF_3$ square plates are enclosed by the {101} and {010} faces and are of size $(130.0 \pm 4.9) \times (75.0 \pm 2.5)$ and $(250.0 \pm 9.5) \times (180.0 \pm 5.5)$ nm^2, respectively (Figure 2c, d and Figure 2e, f). Figure 3 illustrates the 1D growth of the single-crystalline $NaMgF_3$ nanorods. The HRTEM image in Figure 3, inset reveals interplanar distances of 0.34 and 0.54 nm attributed to the {111} and {010} faces, respectively. The preferred growth direction of the $NaMgF_3$ nanorods was determined to be along the [010] direction.

Characterization of $LiMAlF_6$ Nanocrystals

Figure 4 shows the XRD patterns and TEM images of the $LiMAlF_6$ (M = Ca, Sr) nanocrystals. As seen in Figure 4a, the synthesized $LiMAlF_6$ nanocrystals take on a purely hexagonal structure (space group: $P\bar{3}1c$). The calculated lattice constants are as follows: $a = 4.95(1)$ Å and $c = 9.55(6)$ Å for $LiCaAlF_6$ (JCPDS: 43–1481), and $a = 5.09(0)$ Å and $c = 10.28(1)$ Å for $LiSrAlF_6$ (JCPDS: 48–1640). Figure 4b and c shows the formation of uniform $LiCaAlF_6$ and $LiSrAlF_6$ polygons of size (28.4 ± 5.6) and (31.5 ± 3.5) nm, respectively.

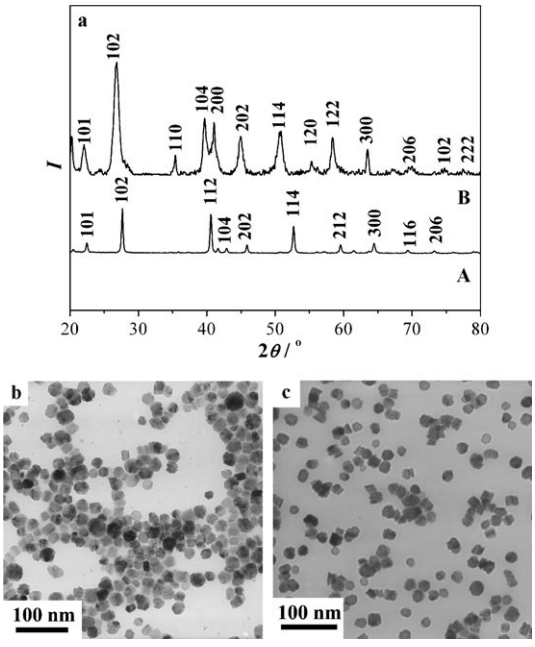

Figure 4. a) XRD patterns of hexagonal $LiCaAlF_6$ (A) and $LiSrAlF_6$ (B) nanocrystals. b) TEM image of $LiCaAlF_6$ nanocrystals. c) TEM image of $LiSrAlF_6$ nanocrystals.

Conditions for the Formation of $NaMF_3$ and $LiMAlF_6$ Nanocrystals

As is well-known, $NaMF_3$ (M = Mn, Co, Ni, Mg) compounds in the $A^IM^{II}F_3$ family are usually of the orthorhombic perovskite structure in space group *Pnma* ($GdFeO_3$-type, $Z = 4$),[15] whereas $LiMAlF_6$ (M = Ca, Sr) in the $LiM^{II}M^{III}F_6$ family crystallize as a trigonal structure in space group $P\bar{3}1c$.[10d] In this work, to uncover the optimal conditions for the formation of phase-pure and monodispersed $NaMF_3$ and $LiMAlF_6$ nanocrystals, we carried out a set of experiments to investigate the effects of different parameters, including the ratios of metals, solvent composition, reaction temperature and time, and precursor concentration, on the particle characteristics of the synthetic products. We found that solvent composition, reaction temperature, and reaction time are three key factors for the synthesis of high-quality nanocrystals.

Solvent Composition

It seems that the use of a combined solvent (either OA/ODE or OA/OM/ODE) is essential for the preparation of phase-pure and monodispersed $NaMF_3$ and $LiMAlF_6$ nanocrystals, whereas the presence of OA ligands in the combined solvent is a prerequisite for phase-pure products (see Supporting Information, Tables S1 and S2). We found that the cothermolysis of $Na(CF_3COO)$ and $M(CF_3COO)_2$ in pure ODE yielded products that contain no $NaMF_3$, whereas in OM/ODE, only ill-shaped particles of NaF and MO (M = Mn, Co, Mg) or Ni_3C were separated from the reaction mixture (Figure 5). In the case of $NaMnF_3$, to obtain pure orthorhombic monodiperse nanocrystals, the combined use of OA/OM/ODE in an appropriate ratio is necessary in the synthesis. For example, by using 1 mmol $Na(CF_3COO)$ and 1 mmol $Mn(CF_3COO)_2$ as the precursors, the reaction in 1:1 OA/ODE at 280 °C for 30 min produced nonuniform $NaMnF_3$ nanoplates with the large size of (119.5–80.3) × (79.7–30.2) nm^2 (Figure 6a), whereas in OA/OM/ODE (4:1:5), near-monodispersed $NaMnF_3$ nanoplates of size $(110.0 \pm 9.5) \times (40.5 \pm 2.0)$ nm^2 were formed (Figure 2a). When more OM was added to attain an OA/OM/ODE ratio of 2:1:3, the size of the monodispersed $NaMnF_3$ nanoplates was decreased to $(68.2 \pm 5.5) \times (30.5 \pm 1.7)$ nm^2 (Table S1). However, when the amount of OM was increased such that OA/OM/ODE = 1:1:2, the $NaMnF_3$ products appeared as a mixture of nanoplates and nanobelts (Figure 6b). These results strongly suggest that monodispersed $NaMnF_3$ nanoplates can only be obtained in the ternary solvent OA/OM/

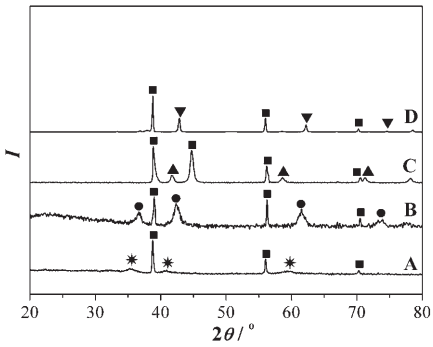

Figure 5. XRD patterns of the products obtained from the cothermolysis of 1 mmol $Na(CF_3COO)$ and 1 mmol $M(CF_3COO)_2$ (M = Mn (A), Co (B), Ni (C), Mg (D)) in OM/ODE (1:1) at 300 °C for 30 min. ■ = NaF, * = MnO, ● = CoO, ▲ = Ni_3C, ▼ = MgO.

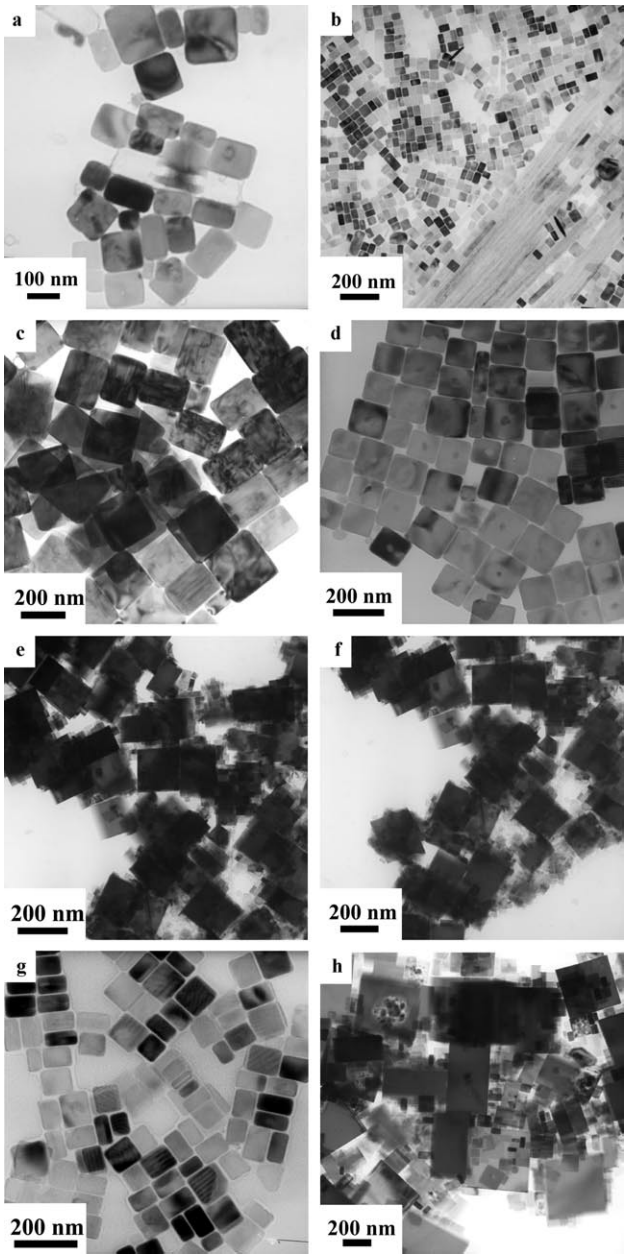

Figure 6. TEM images of orthorhombic $NaMnF_3$ nanoplates obtained from the cothermolysis of 1 mmol $Na(CF_3COO)$ and 1 mmol $Mn(CF_3COO)_2$ under different conditions: a) OA/ODE = 1:1, 280 °C, 30 min; b) OA/OM/ODE = 1:1:2, 280 °C, 30 min; c) OA/OM/ODE = 4:1:5, 310 °C, 30 min; d) OA/OM/ODE = 4:1:5, 260 °C, 30 min; e) OA/OM/ODE = 4:1:5, 280 °C, 15 min; f) OA/OM/ODE = 4:1:5, 280 °C, 0 min; g) OA/OM/ODE = 4:1:5, 280 °C, 45 min; h) OA/OM/ODE = 4:1:5, 280 °C, 60 min.

ODE within a narrow composition range (4:1:5–1:1:2). As for $NaCoF_3$, $NaNiF_3$, $NaMgF_3$, and $LiMAlF_6$ (M = Ca, Sr), high-quality nanocrystals were prepared in the combined solvents of much narrower composition range (OA/ODE = 1:1 and/or OA/OM/ODE = 1:1:2) (Tables S1 and S2).

Reaction Temperature and Time

Using the optimal solvent composition for obtaining phase-pure products, we found that both the reaction temperature and time markedly affect the size distribution of the nanocrystals. For example, at 310 °C, the cothermolysis of 1 mmol $Na(CF_3COO)$ and 1 mmol $Mn(CF_3COO)_2$ in OA/OM/ODE (4:1:5) for 30 min produced near-uniform $NaMnF_3$ nanoplates with a large size of $(223.8 \pm 11.6) \times (180.3 \pm 8.5)$ nm^2 (Figure 6c). As the reaction temperature was decreased to 280 °C, near-monodispersed $NaMnF_3$ nanoplates with the smaller size of $(110.0 \pm 9.5) \times (40.5 \pm 2.0)$ nm^2 were obtained (Figure 2a). When the reaction temperature was further decreased to 270 °C, the size of the nanoplates was slightly decreased to $(109.4 \pm 7.5) \times (37.5 \pm 3.4)$ nm^2. However, the reaction at 250 °C resulted in nonuniform $NaMnF_3$ nanoplates in the size range (158.7–94.9) × (105.5–90.2) nm^2 and in low yield (Figure 6d), possibly due to unfinished thermolysis of the precursors at this low temperature. These results strongly suggest that the growth of the $NaMnF_3$ nanoplates is rather sluggish below 270 °C, but is greatly accelerated at over 280 °C. Under these conditions, the narrowing of the size distribution for the $NaMnF_3$ nanoplates was realized after reaction for 30 min at high temperatures (≥270 °C) by the temperature-driven "size-focusing" process.[1h]

Under the fixed reaction temperature of 280 °C, as the reaction time was shortened from 30 min to 15 and 0 min, highly polydispersed $NaMnF_3$ nanoplates were obtained (Figure 6e and f), thus indicating that a quick "size-focusing" process happened 15–30 min into the reaction.[1h] When the reaction went on for 45 min, the nanoplates were still monodispersed, but with a slightly smaller size of $(108.3 \pm 8.5) \times (50.5 \pm 4.4)$ nm^2 (Figure 6g). However, as the reaction time reached 60 min, $NaMnF_3$ nanoplates with a much broader size distribution were again formed, which suggests that a drastic "size-defocusing" process occurred 45–60 min into the reaction (Figure 6h).[1h] Therefore, these results demonstrate that an Ostwald-ripening process exists in the formation of monodispersed $NaMnF_3$ nanoplates at 280 °C.[1h]

Finally, we found that high-quality stoichiometric $NaMF_3$ and $LiMAlF_6$ nanocrystals can be obtained in an appropriate combined solvent (OA/OM/ODE or OA/ODE) at high temperature over a short reaction time under a relatively high alkali metal/other metals ratio (Tables S1 and S2), due to the well-maintained balance between the nucleation and growth stages under these conditions. However, we noticed that the conditions for the formation of uniform $LiMAlF_6$ nanocrystals were more rigorous than those for $NaMF_3$, possibly due to the greater difficulty in homogeneous nucleation from three trifluoroacetates rather than two during the thermolysis process. $LiMAlF_6$ nanocrystals could only grow uniformly under certain experimental conditions, and usually showed a wider size distribution than the $NaMF_3$ nanocrystals (Tables S1 and S2).

Reaction Pathways for the Formation of $NaMF_3$ Nanocrystals

Through many characterization methods, the reaction pathways for the formation of complex metal fluoride nanocrystals by the cothermolysis of trifluoroacetate precursors in hot surfactant solutions were carefully studied in this work. On the basis of a series of synthesis results for the formation of $NaMF_3$ nanocrystals in both OA/ODE and OA/OM/ODE systems, we suggest the following reaction scheme, which includes two major stages (Scheme 1).

In the first stage, solid powders of $Na(CF_3COO)$ and $M(CF_3COO)_2$ were dissolved in OA/ODE (1:1) under Ar atmosphere upon heating to 100–200 °C. Under these conditions, a pellucid solution appeared with the formation of the reaction intermediates $Na(CF_3COO)_{(1-x)}(OA)_x$/$M(CF_3COO)_{(2-y)}(OA)_y$ and CF_3COO^- ligands in the liquid phase through the exchange reaction between CF_3COO^- and oleate ligands (Scheme 1). This hypothesis was confirmed by FTIR spectroscopy. For example, a transparent solution was formed by dissolving some $Ni(CF_3COO)_2$ in OA/ODE (1:1) at around 140 °C, whose FTIR spectrum is shown in Figure S2 of the Supporting Information. The presence of a strong alkyl C–H stretching band at 2930 cm^{-1} and a carbonyl peak at 1712 cm^{-1} indicates the existence of a large amount of free oleic acid in the solution. However, the broad peak at 1465 cm^{-1} assigned to carboxylate (COO^-) stretching[16] implies an exchange between OA and CF_3COO^- (Figure S2). Further experiments revealed that, with the same reaction temperature and time, the addition of some OM into OA/ODE facilitated the formation of the reaction intermediate partially substituted with oleylamine, that is, $M(CF_3COO)_{(2-y-z)}(OA)_y(OM)_z$ (Scheme 1), due to the strong affinity of the amine groups to the transition metals.[6a,17] This reaction was accompanied by a color change of

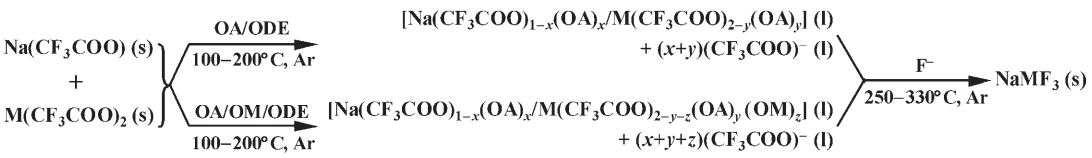

Scheme 1. Reaction pathways for the formation of $NaMF_3$ nanocrystals in hot OA/ODE and OA/OM/ODE. *x* and *y* denote the number of OA molecules involved in the reaction, *z* denotes the number of OM molecules involved.

the solution from pistachio to ultramarine. UV/Vis spectroscopy demonstrated that, in the case of $Ni(CF_3COO)_2$ dissolved in OA/ODE (1:1) at 140 °C, the addition of some oleylamine (OA/OM/ODE = 4:1:5) produced a color variation that appeared as a marked blue shift from 640 to 600 nm (see Supporting information, Figure S3).

In the second stage, F^- ions were produced due to cleavage of the C–F bonds of the CF_3COO^- ligands in solution.[14e,g,h,18] Promptly, solid $NaMF_3$ nuclei were generated by the fluorination of the M–O bonds of $Na(CF_3COO)_{(1-x)}(OA)_x/M(CF_3COO)_{(2-y)}(OA)_y$ or $Na(CF_3COO)_{(1-x)}(OA)_x/M(CF_3COO)_{(2-y-z)}(OA)_y(OM)_z$ with the highly active F^- ions released (Scheme 1). This was deduced from the GC–MS spectra of the components from the cothermolysis of $Na(CF_3COO)$ and $Ni(CF_3COO)_2$ precursors at 180 °C in OA/ODE (1:1) (see Supporting Information, Figure S4). The peaks at $m/z = 69$ and 51 in the mass spectrum of the low-molecular-weight component can be ascribed to the fragments CF_3^+ and CF_2H^+, respectively. The formation of CF_2H^+ should be accompanied by the release of F^- ions. With the nuclei formed, high-quality $NaMF_3$ nanocrystals were harvested by maintaining the balance between the nucleation and growth stages through adjustment of the experimental parameters. However, we noted that the formation of $NaMF_3$ was not induced by the simultaneous nucleation of NaF and MF_2; rather, NaF first separated out from the reaction medium. When the reaction temperature and time were increased, the amount of separated NaF diminished, leading to the final formation of pure $NaMF_3$. For example, with 1 mmol $Na(CF_3COO)$ and 1 mmol $Ni(CF_3COO)_2$ as the precursors in OA/ODE (1:1), NaF was the predominant product formed by reaction at 260 °C for 0 min, but pure $NaNiF_3$ was produced by the reaction at 280 °C for 15 min (Figure 7).

We also noticed that the formation of the reaction intermediate partially substituted with oleylamine by the addition of a suitable amount of OM was very helpful in the size-controlled synthesis of $NaMF_3$ nanoplates (Table S1). However, the existence of redundant OM ligands in OA/ODE (if OM/OA > 1) markedly retarded the growth of $NaMF_3$ nanocrystals; ill-shaped nanocrystals with NaF and MO/M_xC impurities were thus produced (Figure 5). We considered here that OM may play dual and contradictory roles in the whole reaction: one is to promote the formation of $NaMF_3$ by accelerated fluorination between the transition-metal intermediate partially substituted with oleylamine and F^-, the other is to restrict the reactivity of F^- ions due to the strong fluorophilicity of the free oleylamine ligands.[14h,17] For instance, for the cothermolysis of 1 mmol $Na(CF_3COO)$ and 1.2 mmol $Ni(CF_3COO)_2$ at 250 °C for 0 min, no $NaNiF_3$ products were formed in OA/ODE (1:1), but small $NaNiF_3$ nanoplates were produced by the introduction of some OM into OA/ODE (OA/OM/ODE = 4:1:5). This result indicates that the presence of an appropriate amount of OM promotes the formation of $NaNiF_3$. Further experiments showed that too much OM in the solution greatly lowers the reactivity of F^- ions, which consequently holds back the formation of $NaMF_3$ nanocrystals. A good case in point is the emergence of $NaNiF_3$ nanocrystals: if the concentration of OM exceeds a certain value (i.e., OM/OA > 1), NaF would separate out from the reaction medium, and the Ni species partially substituted with oleylamine would be converted into Ni_3C instantly, partly due to the nature of its catalysis (Figure 5).[19] Moreover, to avoid the formation of by-products in the nanocrystal synthesis, a low ratio of OM/OA was required at high reaction temperature.

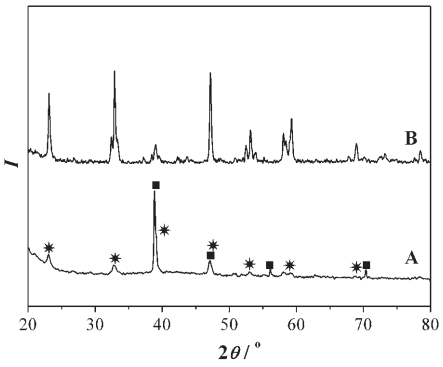

Figure 7. XRD patterns of the products obtained from the cothermolysis of 1 mmol $Na(CF_3COO)$ and 1 mmol $Ni(CF_3COO)_2$ under different conditions: A) OA/ODE = 1:1, 260 °C, 0 min; B) OA/ODE = 1:1, 280 °C, 15 min. ■ = NaF, * = $NaNiF_3$.

Shape Evolution and Size Control of $NaMF_3$ Nanocrystals

The shape evolution of colloidal inorganic nanocrystals is currently of wide interest.[1h,3a] Normally, the crystal shape of inorganic nanocrystals is determined by several factors, including the crystalline phase of the nuclei, the selective adsorption of surfactant onto specific crystal planes, and the balance between kinetic and thermodynamic growth regimes.[1h] Nuclei with an anisotropic crystal structure can grow into anisotropic nanocrystals very easily in the solution phase. In this work, all the $NaMF_3$ (M = Mn, Co, Ni, Mg) compounds have the same orthorhombic perovskite structure, which is anisotropic. Therefore, as expected, we obtained anisotropic $NaMF_3$ nanocrystals: 2D quasisquare nanoplates with confined growth of the {010} faces (M = Mn, Co, Ni) and 1D nanorods with a preferred growth direction of [010] (M = Mg). Given that carboxy groups generally show much stronger coordination to transition-metal ions than to alkali-metal and alkaline-earth-metal ions in solution,[17] we suggest that the formation of a 2D growth structure for the $NaMF_3$ nanocrystals could be due to the selective adsorption of oleate ligands onto the {010} faces, based on the strong binding between the transition-metal ions and the carboxy groups of the oleates. As a result, the growth of the {010} faces was markedly restrained so that {010}-confined $NaMF_3$ nanoplates were formed. Logically, the more OA added, the larger the ratio of edge length to thickness for the nanoplates. For instance, the ratio of edge length to thickness for the $NaMnF_3$ nanoplates increased from 2.2 in OA/OM/ODE = 2:1:3 to 2.7 in OA/OM/ODE = 4:1:5 (Na/

Mn = 1, 280 °C, 30 min; see Table S1). As the alkaline-earth metal replaced the transition metal in the synthesis, $NaMgF_3$ nanocrystals grew highly anisotropically along the [010] direction, owing to the fact that the carboxy groups of the oleates show much weaker coordination with Mg^{2+} ions than with Mn^{2+}, Co^{2+}, or Ni^{2+} ions.[17] Hence, the unrestrained growth along the [010] direction led to the formation of $NaMgF_3$ nanorods.

The crystallite size of the $NaMF_3$ nanocrystals obtained was easily tuned mainly by changing the reaction temperature and time as well as the solvent composition (Figure 8; see also Supporting Information, Figures S5 and S6). For instance, with 1 mmol $Na(CF_3COO)$ and 1 mmol $Mn(CF_3COO)_2$ as the precursors in OA/OM/ODE = 1:1:2, the reaction at 310 °C for 45 min produced $NaMnF_3$ nanoplates of size $(38.5 \pm 2.5) \times (22.5 \pm 0.8)$ nm^2 (Figure 8a), but the reaction at 330 °C for 30 and 45 min yielded larger nanoplates of size $(55.5 \pm 4.5) \times (30.0 \pm 1.8)$ nm^2 (Figure 8b) and $(65.0 \pm 4.5) \times (30.5 \pm 2.1)$ nm^2 (Figure 8c), respectively. In OA/OM/ODE = 4:1:5 at 280 °C for 30 min, uniform $(110.0 \pm 9.5) \times (40.5 \pm 2.0)$ nm^2 nanoplates were obtained (Figure 2a), whereas in OA/ODE = 1 at 330 °C for 120 min, much larger nanoplates of size $(198.0 \pm 4.5) \times (150.5 \pm 2.1)$ nm^2 (Figure 8d) were formed.

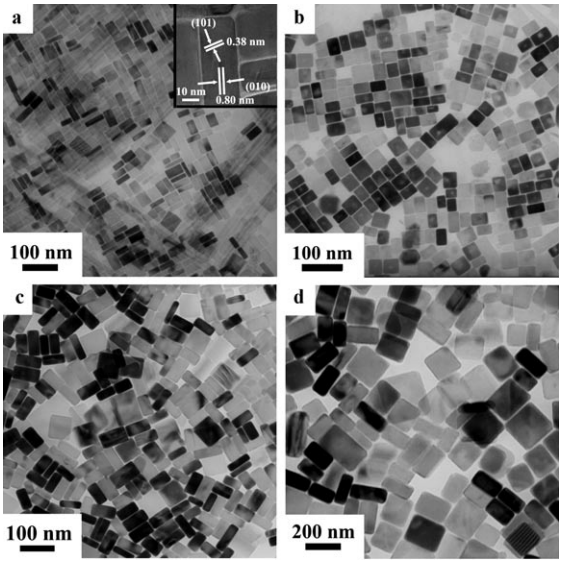

Figure 8. TEM and HRTEM (inset) images of differently sized $NaMnF_3$ nanoplates: a) $(38.5 \pm 2.5) \times (22.5 \pm 0.8)$ nm^2; b) $(55.5 \pm 4.5) \times (30.0 \pm 1.8)$ nm^2; c) $(65.0 \pm 4.5) \times (30.5 \pm 2.1)$ nm^2; d) $(198.0 \pm 4.5) \times (83.8 \pm 2.1)$ nm^2.

Magnetic Behavior of $NaMnF_3$ Nanoplates

Previously, it was reported that bulk $NaMnF_3$, $NaCoF_3$, and $NaNiF_3$ generally present weak ferromagnetic properties with antiferromagnetic interactions with Néel transition temperatures (T_N) of 66,[20] 77,[21] and 150 K,[22] respectively. As these compounds are important magnetic model systems, it is interesting to investigate their magnetic interaction and ordering state when their sizes shrink to nanometer dimensions, owing to the exchange interaction induced by the surface chemical bonds or lattice stress. However, because of the difficulty in the synthesis of their monodispersed nanocrystals, there have been few reports on the magnetic behavior of these materials on the nanometer scale.[11b]

Herein, we discuss the magnetic properties of $NaMnF_3$ nanoplates of different sizes. Figure 9a–d shows the temperature dependence of the magnetic susceptibility (M–T) behavior of $NaMnF_3$ nanoplates of size $(198.0 \pm 4.5) \times (150.5 \pm 2.1)$, $(110.0 \pm 9.5) \times (40.5 \pm 2.0)$, $(55.5 \pm 4.5) \times (30.0 \pm 1.8)$, and $(38.5 \pm 2.5) \times (22.5 \pm 0.8)$ nm^2, respectively. The observed T_N values are around 68–70 K for the former three samples, which coincides with the corresponding bulk compound, and show no significant shifts. This result indicates the similar antiferromagnetic interaction mode among these three samples and bulk $NaMnF_3$. Moreover, the large difference between the zero-field-cooling (ZFC) and field-cooling (FC) plots and the dependence of FC susceptibility on nanocrystal size imply the weak ferromagnetic behavior of the synthesized $NaMnF_3$ nanoplates, especially for those of size $(198.0 \pm 4.5) \times (150.5 \pm 2.1)$ and $(110.0 \pm 9.5) \times (40.5 \pm 2.0)$ nm^2 (Figure 9a and b, respectively). However, when the nanoplate size drops to $(55.5 \pm 4.5) \times (30.0 \pm 1.8)$ and $(38.5 \pm 2.5) \times (22.5 \pm 0.8)$ nm^2, we observed a sharply increased magnetic moment at around 11 K (Figure 9c and d), possibly due to the noncompensation of the surface spins.[11] In particular, for the smallest nanoplates, the increase in the magnetic moment was more significant and the T_N value decreased to 40 K (Figure 9d), thus indicating the strong surface effect of the nanoplates.[11]

Upconversion Luminescence of $NaMgF_3$:Yb,Er Nanorods

The design and characterization of new upconversion (UC) luminescent materials is an active area of research.[23] Using the cothermolysis of multiple metal (Na, Mg, Yb, and Er) trifluoroacetates in OA/ODE (1:1) at 300 °C for 45 min, we obtained $NaMgF_3$:20 % Yb,2 % Er nanorods, which showed a strong red emission under 980-nm near-IR excitation. To the best of our knowledge, there has not yet been a report on the UC properties of rare-earth-doped $NaMgF_3$.

The $NaMgF_3$:20 % Yb,2 % Er nanorods prepared have an orthorhombic structure (Figure 10a) with the lattice parameters $a = 5.40(6)$, $b = 5.52(1)$, $c = 7.80(8)$ nm (space group: *Pnma*). The expansion of the lattice constants from $NaMgF_3$ to $NaMgF_3$:20 % Yb,2 % Er nanorods testifies to the successful co-doping of the Yb^{3+} and Er^{3+} ions into the crystal lattice of $NaMgF_3$. As seen in Figure 10b, the nanorods have a relatively uniform width, and are $(337.2–66.3) \times (10.3 \pm 1.6)$ nm^2 large.

Figure 10c shows the room-temperature UC fluorescence spectrum of the colloidal $NaMgF_3$:20 % Yb,2 % Er nanorods redispersed in cyclohexane under 980-nm near-IR excitation. The three characteristic emission peaks at 525, 552, and 662 nm are assigned to the $^2H_{11/2} \rightarrow {}^4I_{15/2}$, $^4S_{3/2} \rightarrow {}^4I_{15/2}$, and $^4F_{9/2}$

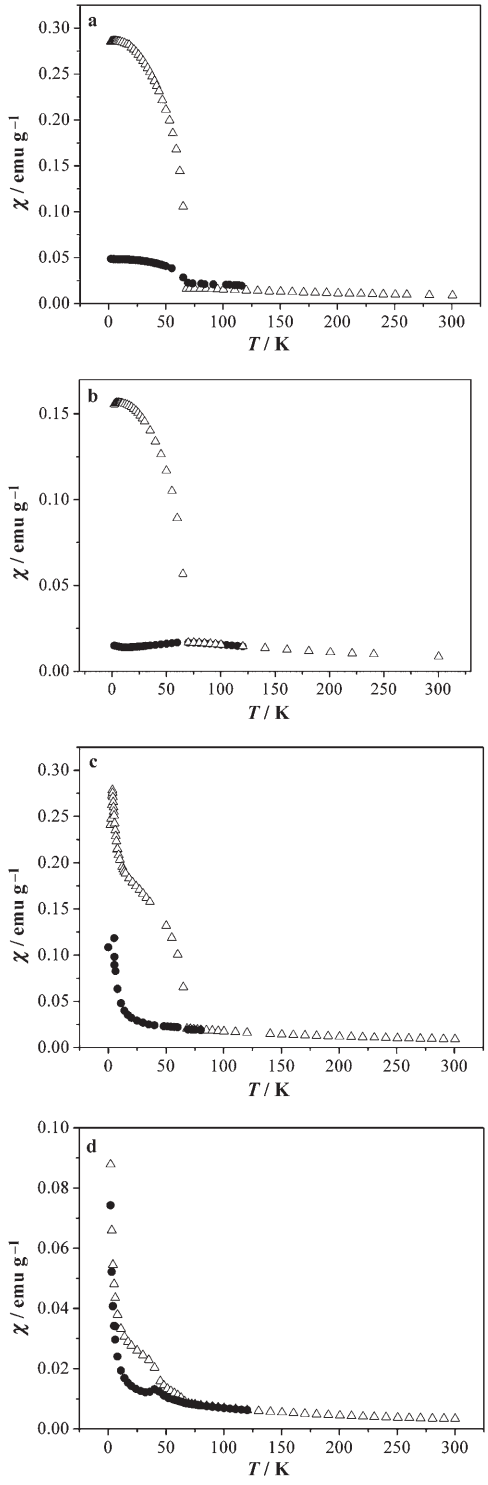

Figure 9. ZFC (△) and FC (●) magnetization curves of differently sized $NaMnF_3$ nanoplates with an applied field of 100 Oe: a) (198.0 ± 4.5) × (150.5 ± 2.1) nm^2; b) (110.0 ± 9.5) × (40.5 ± 2.0) nm^2; c) (55.5 ± 4.5) × (30.0 ± 1.8) nm^2; d) (38.5 ± 2.5) × (22.5 ± 0.8) nm^2.

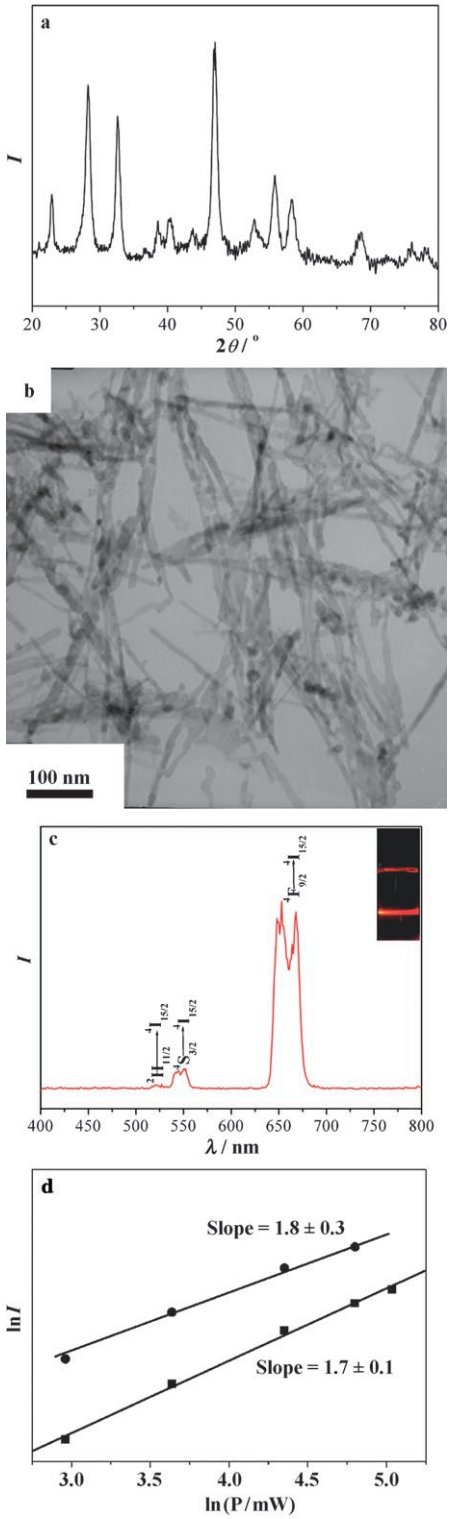

Figure 10. a) XRD pattern and b) TEM image of $NaMgF_3$:20 % Yb,2 % Er nanorods. c) Room-temperature upconversion fluorescence spectrum of $NaMgF_3$:20 % Yb,2 % Er nanorods dispersed in cyclohexane (0.05 mol L^{-1}); inset: photograph of the dispersion under 980-nm near-IR excitation. d) Power dependence of the upconversion emission of $NaMgF_3$:20 % Yb,2 % Er nanorods dispersed in cyclohexane under 980-nm near-IR excitation; ■ = $^4S_{3/2} \rightarrow {}^4I_{15/2}$, ● = $^4F_{9/2} \rightarrow {}^4I_{15/2}$.

$\rightarrow {}^4I_{15/2}$ transitions of erbium, respectively. The strong red emissions located at 652 and 662 nm resulting from the same transition ($^4F_{9/2} \rightarrow {}^4I_{15/2}$) hint that the synthesized $NaMgF_3$:20 % Yb,2 % Er nanorods may be a good candidate

for red UC materials. From the plots of the power dependence of the UC emissions for the nanorods (Figure 10d), the slopes for both green and red emissions were determined to be approximately two. Therefore, we consider the two-photon process as the upconversion mechanism, as shown in Equations (1)–(3), in which ET is energy transfer (see also Supporting Information, Figure S7).[24]

$$^2F_{7/2}(Yb^{3+}) \xrightarrow{980nm} {}^2F_{5/2}(Yb^{3+}) \quad (1)$$

$$^2F_{5/2}(Yb^{3+}) + {}^4I_{11/2}(Er^{3+}) \xrightarrow{ET} {}^2F_{5/2}(Yb^{3+}) + {}^4F_{7/2}(Er^{3+}) \quad (2)$$

$$^4F_{7/2}(Er^{3+}) \xrightarrow{relaxation} {}^2H_{11/2}(Er^{3+}) \xrightarrow{relaxation} {}^4F_{9/2} \xrightarrow{transition} {}^4I_{15/2} \quad (3)$$

Conclusions

Single-crystalline and near-monodispersed $NaMF_3$ (M = Mn, Co, Ni, Mg), $LiMAlF_6$ (M = Ca, Sr), and $NaMgF_3$:Yb,Er nanocrystals (quasisquare nanoplates, nanorods, and nanopolygons) were synthesized by the cothermolysis of multiple trifluoroacetates in hot high-boiling-point solvents. By simply tuning the synthetic parameters such as reaction temperature and time and solvent composition, we could manipulate the size of the $NaMF_3$ nanocrystals. The narrow size distribution of the nanocrystals provided by this method allowed the $NaMF_3$ (M = Mn, Co, Ni) nanocrystals to partially self-assemble into nanoarrays on copper TEM grids. The $NaMnF_3$ square plates prepared showed interesting weak ferromagnetic behavior on the nanoscale, and the $NaMgF_3$:Yb,Er nanorods displayed strong UC red emissions under 980-nm near-IR excitation. We believe that the current work could contribute to diverse research fields related to the synthetic chemistry, magnetic and optical physics, and nanomaterials science of dispersible inorganic nanocrystals (particularly for complex metal fluorides), and thus should be of adequate theoretical and practical interest.

Experimental Section

Chemicals

All the nanocrystals were synthesized by using standard air-free procedures. OA (90%, Alpha), OM (>80%, Acros), ODE (>90%, Acros), trifluoroacetic acid (99%, Acros), $A(CF_3COO)$ (A = Na, K, >97%, Acros), absolute ethanol, hexane, toluene, and cyclohexane were used as received. Precursors such as $M(CF_3COO)_2$ (M = alkaline-earth or transition metal), $Li(CF_3COO)$, and $M(CF_3COO)_3$ (M = Al, Yb, Er) were prepared from the corresponding metal oxides, hydroxides, or carbonates according to the literature method.[18]

Synthesis of $NaMF_3$ (M = Mn, Co, Ni, Mg) Nanocrystals

The typical synthetic procedure is as follows: A given amount of $Na(CF_3COO)$ and $M(CF_3COO)_2$ (M = Mn, Co, Ni, Mg) and OA/OM/ODE (40 mmol) were loaded into a three-necked flask at room temperature to form a slurry, which was then heated to 100–120 °C for 30 min under Ar atmosphere with vigorous magnetic stirring in a temperature-controlled electromantel. The reaction mixture was repeatedly evacuated to remove water and oxygen until a transparent solution was produced, which was then rapidly heated within 10–15 min to 250–330 °C and held at that temperature for the desired length of time. The solution was then cooled to room temperature in air to form a nanocrystal suspension, after which the nanocrystals were retrieved by adding absolute ethanol (50 mL) to the suspension, followed by a centrifugation at 7500 rpm for 15 min. The precipitated nanocrystals were dried overnight in air at 70 °C. The yields of all the nanocrystals afforded without any size sorting were 65–75%. All the prepared nanocrystals were easily redispersed in various nonpolar organic solvents such as hexane, toluene, and cyclohexane.

Synthesis of $NaMgF_3$:20% Yb,2% Er Nanorods

The synthetic procedure was the same as that used to synthesize $NaMgF_3$ nanocrystals, except that $Na(CF_3COO)$ (1 mmol) and stoichiometric amounts of $Mg(CF_3COO)_2$, $Yb(CF_3COO)_3$, and $Er(CF_3COO)_3$ were added to a mixture of OA (20 mmol) and ODE (20 mmol) in a three-necked flask at room temperature for reaction at 300 °C for 45 min.

Synthesis of $LiMAlF_6$ (M = Ca, Sr) Nanocrystals

The synthetic procedure was the same as that used to synthesize $NaMF_3$ nanocrystals, except that $Li(CF_3COO)$, $Al(CF_3COO)_3$, and $M(CF_3COO)_2$ (M = Ca, Sr) (1 mmol each) were added to a mixture of OA (20 mmol) and ODE (20 mmol) in a three-necked flask at room temperature for reaction at 300 °C for 60 min.

Characterization

Powder XRD patterns were recorded on a Rigaku $D/_{MAX}$-2000 diffractometer (Japan) with a slit width of 0.5° at a scanning rate of $2° min^{-1}$ with $Cu_{K\alpha}$ radiation ($\lambda = 1.5418$ Å). Samples for TEM analysis were prepared by slow evaporation of a drop of nanocrystal dispersion in hexane/toluene (1:1 *v*/*v*) on a carbon-coated copper grid. Particle sizes and shapes were determined by a transmission electron microscope (200CX, JEOL, Japan) operating at 160 kV. HRTEM observations and EDAX analysis were carried out on a Philips Tecnai F30 FEG-TEM microscope operating at 300 kV. FTIR spectra were obtained on a Bruker Vector22 spectrophotometer. GC–MS spectra were collected with a USA Finnigan-MAT GCQ gas chromatograph/mass spectrometer. The upconversion fluorescence spectrum of $NaMgF_3$:20% Yb,2% Er nanorods dispersed in cyclohexane ($0.05 mol L^{-1}$) was recorded at room temperature by using a modified Hitachi F-4500 spectrophotometer with an external 980-nm laser diode as the excitation source in place of the xenon lamp in the spectrometer. Magnetic susceptibilities were measured by using a Quantum Design USA MPMS-XL-5 superconductive quantum interference device (SQUID) magnetometer from 5 to 300 K with a measuring field of 100 Oe. The temperature dependence of the susceptibility was investigated by cooling the dried sample at zero field and then stepping up the temperature (ZFC curve), or by cooling the sample in the presence of an external field (FC curve). Both curves were collected with an applied field of 100 Oe.

Acknowledgements

We gratefully acknowledge financial aid from the MOST of China (grant no. 2006CB601104), the NSFC (grant nos. 20571003, 20221101, and 20423005), and the Research Fund for the Doctoral Program of Higher Education of the MOE of China (grant no. 20060001027).

[1] a) C. B. Murray, D. J. Norris, M. G. Bawendi, *J. Am. Chem. Soc.* **1993**, *115*, 8706–8715; b) A. P. Alivisatos, *Science* **1996**, *271*, 933–937; c) M. Bruchez, Jr., M. Moronne, P. Gin, S. Weiss, A. P. Alivisatos, *Science* **1998**, *281*, 2013–2016; d) S. H. Sun, C. B. Murray, D. Weller, L. Folks, A. Moser, *Science* **2000**, *287*, 1989–1992; e) V. F. Puntes, K. M. Krishnan, A. P. Alivisatos, *Science* **2001**, *291*, 2115–2117; f) N. R. Jana, X. G. Peng, *J. Am. Chem. Soc.* **2003**, *125*, 14280–14281; g) J. Park, K. An, Y. Hwang, J.-G. Park, H.-J. Noh, J.-Y. Kim,

J.-H. Park, N.-M. Hwang, T. Hyeon, *Nat. Mater.* **2004**, *3*, 891–895; h) Y. Yin, A. P. Alivisatos, *Nature* **2005**, *437*, 664–670.
[2] a) T. S. Ahmadi, Z. L. Wang, T. C. Green, A. Henglein, M. A. El-Sayed, *Science* **1996**, *272*, 1924–1926; b) J. W. Stouwdam, F. C. J. M. van Veggel, *Nano Lett.* **2002**, *2*, 733–737; c) M. Yin, S. O'Brien, *J. Am. Chem. Soc.* **2003**, *125*, 10180–10181; d) T. Yu, J. Joo, Y. I. Park, T. Hyeon, *J. Am. Chem. Soc.* **2006**, *128*, 1786–1787.
[3] a) X. G. Peng, L. Manna, W. D. Yang, J. Wickham, E. Scher, A. Kadavanich, A. P. Alivisatos, *Nature* **2000**, *404*, 59–61; b) J. J. Li, Y. A. Wang, W. Z. Guo, J. C. Keay, T. D. Mishima, M. B. Johnson, X. G. Peng, *J. Am. Chem. Soc.* **2003**, *125*, 12567–12575.
[4] Y. G. Sun, Y. N. Xia, *Science* **2002**, *298*, 2176–2179.
[5] C. Desvaux, C. Amiens, P. Fejes, P. Renaud, M. Respaud, P. Lecante, E. Snoeck, B. Chaudret, *Nat. Mater.* **2005**, *4*, 750–753.
[6] a) J. Park, E. Kang, S. U. Son, H. M. Park, M. K. Lee, J. Kim, K. W. Kim, H.-J. Noh, J.-H. Park, C. J. Bae, J.-G. Park, T. Hyeon, *Adv. Mater.* **2005**, *17*, 429–434; b) M. Yin, C.-K. Wu, Y. Lou, C. Burda, J. T. Koberstein, Y. Zhu, S. O'Brien, *J. Am. Chem. Soc.* **2005**, *127*, 9506–9511; c) R. Si, Y.-W. Zhang, L.-P. You, C.-H. Yan, *Angew. Chem.* **2005**, *117*, 3320–3324; *Angew. Chem. Int. Ed.* **2005**, *44*, 3256–3260.
[7] A. H. Cooke, D. A. Jones, J. F. A. Silva, M. R. Weils, *J. Phys. C: Solid State Phys.* **1975**, *8*, 4083–4088.
[8] R. A. Heaton, C. C. Lin, *Phys. Rev. B* **1982**, *25*, 3538–3549.
[9] M. Eibschutz, H. J. Guggenheim, *Solid State Commun.* **1968**, *6*, 737–739.
[10] a) A. Meijerink, *J. Lumin.* **1993**, *55*, 125–138; b) A. V. Gektin, I. M. Krasovitskaya, N. V. Shiran, *J. Lumin.* **1997**, *72–74*, 664–666; c) Y. W. Tan, C. S. Shi, *J. Solid State Chem.* **2000**, *150*, 178–182; d) T. A. Samtleben, J. Hulliger, *Opt. Laser Eng.* **2005**, *43*, 251–262.
[11] a) F. Agnoli, W. L. Zhou, C. J. O'Connor, *Adv. Mater.* **2001**, *13*, 1697–1699; b) C. J. O'Connor, V. Kolesnichenko, E. Carpenter, C. Sangregorio, W. L. Zhou, A. Kumbhar, J. Sims, F. Agnoli, *Synth. Met.* **2001**, *122*, 547–557.
[12] G. D. Dzik, I. Sokolska, S. Golab, M. Baluka, *J. Alloys Compd.* **2000**, *300*, 254–260.
[13] a) S. L. Zhao, Y. B. Hou, X. J. Pei, Z. Xu, X. R. Xu, *J. Alloys Compd.* **2004**, *368*, 298–303; b) Q. Tang, J. W. Shen, W. J. Zhou, J. W. Liu, Z. P. Liu, Y. T. Qian, *Inorg. Chem. Commun.* **2004**, *7*, 283–285; c) B. Huang, J.-M. Hong, X.-T. Chen, Z. Yu, X.-Z. You, *Mater. Lett.* **2005**, *59*, 430–433.
[14] a) W. W. Yu, X. G. Peng, *Angew. Chem.* **2002**, *114*, 2474–2477; *Angew. Chem. Int. Ed.* **2002**, *41*, 2368–2371; b) V. F. Puntes, D. Zanchet, C. K. Erdonmez, A. P. Alivisatos, *J. Am. Chem. Soc.* **2002**, *124*, 12874–12880; c) E. V. Shevchenko, D. V. Talapin, H. Schnablegger, A. Kornowski, O. Festin, P. Svedlindh, M. Haase, H. Weller, *J. Am. Chem. Soc.* **2003**, *125*, 9090–9101; d) W. S. Seo, J. H. Shim, S. J. Oh, E. K. Lee, N. H. Hur, J. T. Park, *J. Am. Chem. Soc.* **2005**, *127*, 6188–6189; e) Y.-W. Zhang, X. Sun, R. Si, L.-P. You, C.-H. Yan, *J. Am. Chem. Soc.* **2005**, *127*, 3260–3261; f) B. D. Yuhas, D. O. Zitoun, P. J. Pauzauskie, R. R. He, P. D. Yang, *Angew. Chem.* **2006**, *118*, 434–437; *Angew. Chem. Int. Ed.* **2006**, *45*, 420–423; g) H.-X. Mai, Y.-W. Zhang, R. Si, Z.-G. Yan, L.-D. Sun, L.-P. You, C.-H. Yan, *J. Am. Chem. Soc.* **2006**, *128*, 6426–6436; h) X. Sun, Y.-W. Zhang, Y.-P. Du, Z.-G. Yan, R. Si, L.-P. You, C.-H. Yan, *Chem. Eur. J.* **2007**, *13*, 2320–2332.
[15] B. Lütgert, D. Babel, *Z. Anorg. Allg. Chem.* **1992**, *616*, 133–140.
[16] A. L. Willis, N. J. Turro, S. O'Brien, *Chem. Mater.* **2005**, *17*, 5970–5975.
[17] J. A. Dean, *Lange's Handbook of Chemistry*, *15th ed.*, McGraw-Hill, New York, **1999**.
[18] J. E. Roberts, *J. Am. Chem. Soc.* **1961**, *83*, 1087–1088.
[19] Y. H. Leng, H. Y. Shao, Y. T. Wang, M. Suzuki, X. G. Li, *J. Nanosci. Nanotechnol.* **2006**, *6*, 221–226.
[20] J. R. Shane, D. H. Lyons, M. Kestigian, *J. Appl. Phys.* **1967**, *38*, 1280–1282.
[21] Z. Friedman, M. Melamud, J. Makovsky, H. Shaked, *Phys. Rev. B* **1970**, *2*, 179–181.
[22] A. Epstein, J. Makovsky, M. Melamud, H. Shaked, *Phys. Rev.* **1968**, *174*, 560–561.
[23] J. F. Suyver , A. Aebischer, D. Biner, P. Gerner, J. Grimm, S. Heer, K. W. Krämer, C. Reinhard, H. U. Güdel, *Opt. Mater.* **2005**, *27*, 1111–1130.
[24] R. Scheps, *Prog. Quantum Electron.* **1996**, *20*, 271–358.

Received: February 15, 2007
Published online: May 30, 2007

